DRAFT VERSION FEBRUARY 1, 2008
Preprint typeset using LaTeX style emulateapj

FLARING UP ALL OVER — RADIO ACTIVITY IN RAPIDLY-ROTATING LATE M AND L DWARFS

E. BERGER
Division of Physics, Mathematics, and Astronomy, California Institute of Technology 105-24, Pasadena, CA 91125
ejb@astro.caltech.edu

Draft version February 1, 2008

ABSTRACT

We present Very Large Array observations of twelve late M and L dwarfs in the Solar neighborhood. The observed sources were chosen to cover a wide range of physical characteristics — spectral type, rotation, age, binarity, and X-ray and Hα activity — to determine the role of these properties in the production of radio emission, and hence magnetic fields. Three of the twelve sources, TVLM 513-46546, 2MASS J0036159+182110, and BRI 0021−0214, were observed to flare and also exhibit persistent emission, indicating that magnetic activity is not quenched at the bottom of the main sequence. The radio emission extends to spectral type L3.5, and there is no apparent decrease in the ratio of flaring luminosities to bolometric luminosities between M8–L3.5. Moreover, contrary to the significant drop in persistent Hα activity beyond spectral type M7, the persistent radio activity appears to steadily increase between M3–L3.5. Similarly, the radio emission from BRI 0021−0214 violates the phenomenological relations between the radio and X-ray luminosities of coronally active stars, hinting that radio and X-ray activity are also uncorrelated at the bottom of the main sequence; an even stronger violation was found for the brown dwarf LP944-20. The radio active sources that have measured rotational velocities are rapid rotators, $v\sin i > 30$ km sec^{-1}, while the upper limits on radio activity in slowly-rotating late M dwarfs ($v\sin i < 10$ km sec^{-1}) from this survey and from the literature are lower than these detections. These observations provide tantalizing evidence that rapidly-rotating late M and L dwarfs are more likely to be radio active. This possible correlation is puzzling given that the observed radio emission requires sustained magnetic fields of $\sim 10-10^3$ G and densities of $\sim 10^{12}$ cm^{-3}, indicating that the active sources should have slowed down considerably due to magnetic braking.

Subject headings: stars: low mass,brown dwarf–stars: activity–stars: radio emission–stars: magnetic fields–radiation mechanisms: nonthermal

1. INTRODUCTION

Activity in dwarf stars, as measured through the ratios of Hα and X-ray luminosities to bolometric luminosities, drops significantly in spectral types later than M7, and is possibly dominated by flares (Liebert et al. 1999; Reid et al. 1999; Gizis et al. 2000; Kirkpatrick et al. 2000). In addition, the dependence of activity on rotation appears to break down in sources with spectral type later than early-mid M, so that even rapidly rotating sources ($v\sin i \gtrsim 20$ km sec^{-1}) show a decrease in emission (Basri & Marcy 1995; Tinney & Reid 1998) . On the other hand, the transition from a radiative-convective ($\alpha\Omega$) to a turbulent (α^2) dynamo (Durney, De Young & Roxburgh 1993) around the convective mass limit of 0.3 $M_\odot$ (spectral type $\sim$ M3) is not accompanied by a drop in activity (Hawley, Gizis & Reid 1996), indicating that in early M dwarfs the turbulent dynamo can sustain active coronae. It has been suggested that the observed shift to weak flaring activity in late M and L dwarfs is possibly due to a change in the nature of the dynamo, or decreased photospheric ionization levels. If radio activity follows the same pattern, then late M and L dwarfs would exhibit at most only weak flaring, and possibly weaker quiescent radio emission.

In addition, Guedel & Benz (1993), and Benz & Guedel (1994) have shown that for a broad range of coronally active stars (up to spectral type M7) there is a correlation between the radio and X-ray luminosities. Simply, the quiescent luminosities are related by $L_{\rm rad,q} \approx L_{\rm X,q}/10^{15.5}$ Hz^{-1}, while the relation for flaring luminosities is slightly non-linear with $L_{\rm rad,f} \approx L_{\rm X,f}/10^{15.5}$ Hz^{-1} for radio flares with $L_{\rm rad} \sim 10^{14}$ erg sec^{-1} Hz^{-1}. These relations are explained in terms of a heating process in which there is a causal relation between the radio-emitting electrons and the X-ray emitting thermal plasma. The extension of the Guedel–Benz relations to spectral types later than M7 based on X-ray observations (Neuhäuser et al. 1999; Rutledge et al. 2000) predicts radio emission well below the detection limit of the Very Large Array. Past observations seemed to confirm this prediction (Krishnamurthi, Leto & Linsky 1999).

The recent detections of an X-ray flare (Rutledge et al. 2000) and persistent and flaring radio emission (Berger et al. 2001; hereafter B01) from the brown dwarf LP 944-20 (spectral type M9) pose a serious challenge to these ideas, since they demonstrate that late dwarfs can exhibit strong activity closely related to magnetic fields. The quiescent radio emission in particular indicates that the magnetic activity is persistent, contrary to Hα and X-ray observations of this source (Rutledge et al. 2000). Moreover, the observed emission violates both Guedel–Benz relations by approximately four orders of magnitude despite the fact that LP 944-20 is only an M9 source, hinting at a possible breakdown in the relation between radio and X-ray activity between spectral types M7 and M9. Finally, the rapid rotation of LP 944-20, $v\sin i \approx 30$ km sec^{-1}, is puzzling given that the radio emission requires the presence of magnetic fields and ionized material, which should lead to magnetic braking.

These observations raise several crucial questions: Is LP 944-20 a unique object, or do other late-type stars and brown dwarfs

show similar levels of radio activity? What is the underlying mechanism that gives rise to the emission, and is it similar to the mechanism in early M dwarfs? Is the same process responsible for the observed Hα and X-ray flares, and in some cases persistent emission? Is the activity correlated with particular physical properties?

To address these questions, we have undertaken a survey of twelve late-type dwarfs (ranging from M5 through T6) that span a wide range of properties. The purpose of this survey is to search for flaring and/or persistent radio emission, and to investigate whether this emission, and presumably magnetic field production, are correlated with particular physical properties of the sources.

We summarize the properties of the survey sources in §2. The radio observations and data reduction are detailed in §3. In §4 we show that three of the twelve sources exhibit radio emission. We analyze the radio emission, show that at least in one case it violates the Guedel–Benz relations, and estimate the magnetic field strengths and coronal densities in §5. We also discuss the implications for coronal heating mechanisms (§5.3). Finally, in §6 we compare the results of the survey to previous radio surveys of M and L dwarfs, as well as LP944-20, and we draw preliminary conclusions about possible correlations between radio activity and physical parameters.

2. TARGET SELECTION

We observed twelve late M and L dwarfs, two of which are confirmed brown dwarfs, ranging in distance from $\approx 8-160$ pc, and spanning a wide range of ages, rotation, activity, and spectral types. Below and in Table 1 we summarize the main properties of each source in the survey.

CRBR 15: This source is a brown dwarf candidate in the ρ Oph molecular cloud (Wilking, Greene & Meyer 1999). The mass and age of CRBR 15, $M \lesssim 0.1$ M$_\odot$ and $t \lesssim 3$ Myr, are estimated by a comparison to evolutionary models and isochrones (Burrows et al. 1997; Wilking, Greene & Meyer 1999). Wilking et al. (1999) claim that while the age of this source is secure relative to other sources in the ρ Oph cloud, the absolute scale is model-dependent. Still, this source is the youngest in our sample. The temperature and bolometric luminosity of CRBR 15 are estimated at $2900-3000$ K and $\log(L_{\rm bol}/L_\odot) \approx -1.0$ to -1.3 (Luhman & Rieke 1999; Wilking, Greene & Meyer 1999). In a recent observation of the ρ Oph molecular cloud with Chandra (Imanishi, Tsujimoto & Koyama 2001) an upper limit of $L_{\rm X} < 1.1\times10^{28}$ erg sec^{-1} was found for this source, with $\log(L_{\rm X}/L_{\rm bol}) < -4.2$, well below the X-ray saturation limit, $\log(L_{\rm X}/L_{\rm bol}) \approx -3$. In addition, CRBR 15 exhibits excess emission at 2.2 μm (Wilking, Greene & Meyer 1999), and has a flux density of 40 mJy at 1.3 mm (Motte, Andre & Neri 1998). These observations indicate that it is associated with a circumstellar envelope or an accretion disk. Thus, radio emission from this source can be due to accretion or deuterium burning.

LHS 2243: This source is a slowly rotating, $v\sin i < 5$ km sec^{-1}, M8 dwarf. It shows evidence for weak persistent Hα emission, as well as Hα flares, with an increase of ~ 30 in the line equivalent width (Martín, Rebolo & Magazzu 1994; Gizis et al. 2000). The temperature of LHS 2243 is estimated to be ~ 2900 K (Martín, Rebolo & Magazzu 1994) based on the calibration of Kirkpatrick et al. (1993). This calibration provides the highest temperatures among the published temperature conversions (Martín, Rebolo & Magazzu 1994). Bessell (1991) suggested that this source is possibly as young as a few $\times 10^8$ yr, based on its smaller proper motion compared to bluer stars. For an age of $\sim 10^9$ yr, the inferred mass, based on an upper limit on Li abundance and several evolutionary models is $\sim 0.06-0.07$ M$_\odot$ (Martín, Rebolo & Magazzu 1994). If the source is younger than 10^9 yr, the mass would be slightly higher.

TVLM 513-46546: This is a nearby M8.5 dwarf (Tinney 1993; Tinney et al. 1995; Reid et al. 2001). TVLM 513-46546 (hereafter TVLM 513) is the fastest rotator in our sample with $v\sin i \approx 60$ km sec^{-1}, but it has only weak Hα emission with equivalent width of 2.5A (Martín, Rebolo & Magazzu 1994). Based on $1-2.5$ μm spectroscopy, and synthetic spectra fitting, Leggett et al. (2001) find $\log(L_{\rm bol}/L_\odot) \approx -3.65$ and $T \approx 2200$ K for this source. We note however, that their temperature scale provides consistently lower temperatures relative to other estimates (see notes on LHS 2065 below).

LHS 2065: This source has spectral type M9 and relatively slow rotational velocity, $v\sin i \approx 9$ km sec^{-1} (Tinney & Reid 1998; Martín et al. 1999; Reid et al. 2001). It is active in Hα, exhibiting strong flares with a recurrence of < 0.03 hr^{-1}, and possibly more frequent weak flares at a rate ~ 0.5 hr^{-1} (Martín & Ardila 2001). There are several estimates of the effective temperature of this source in the literature, ranging from $2100-2600$ K. Leggett et al. (2001) provide an estimate of 2100 K (see notes on TVLM 513 above). Another estimate, based on near infrared photometry, provides a temperature of 2300 K (Leggett, Allard & Hauschildt 1998; Martín et al. 1999), while Martín, Rebolo & Magazzu (1994) provide a value of 2630 K (see notes on LHS 2243 above). The luminosity of LHS 2065 is estimated to be $\log(L/L_{\rm bol}) \approx -3.5$ (Leggett et al. 2001), and its mass is estimated at $\sim 0.06-0.1$ M$_\odot$ (Martín, Rebolo & Magazzu 1994) which places it close to the brown dwarf cutoff.

BRI 0021–0214: This nearby, M9.5 dwarf is a rapid rotator, $v\sin i \approx 40$ km sec^{-1} (Basri & Marcy 1995; Tinney & Reid 1998), but it exhibits no persistent Hα emission (Tinney & Reid 1998). Reid et al. (1999) discovered an Hα flare from this source, with a peak emission three times lower than the mean quiescent emission of early M dwarfs. In addition, BRI 0021−0214 (hereafter BRI 0021) has an upper limit on X-ray emission of $\log(L_X/L_{\rm bol}) < -4.7$, well below the X-ray saturation limit of $\log(L_X/L_{\rm bol}) \approx -3$ for X-ray active stars (Neuhäuser et al. 1999). Leggett et al. (2001) estimate the temperature of this source at 2100 K, and its luminosity at $\log(L_{\rm bol}/L_\odot) \approx -3.4$. Finally, Martín, Basri & Zapatero Osorio (1999) find an upper limit on Li EW of < 0.08 A. The rapid rotation, flaring emission, and lack of persistent Hα and X-ray emission indicate that this source is an analog of LP 944-20.

PC 0025+0447: This source is possibly a young (< 1 Gyr) brown dwarf (M< 0.06 M$_\odot$; Martín, Basri, & Zapatero Osorio 1999), based on the detection of Li with EW$= 1.0\pm0.3$ A. PC 0025+0447 (hereafter PC 0025) exhibits very strong and persistent Hα emission (Graham et al. 1992; Mould et al. 1994). Burgasser et al. (2000), on the other hand, suggest that PC 0025 is an interacting binary in order to explain the Li and Hα observations. The rotational velocity of PC 0025 is surprisingly low, $v\sin i \approx 13\pm3$ km sec^{-1}, given the strong level of Hα activity. In addition, PC 0025 has an upper limit on X-ray emission of $\log L_{\rm X} < 27.2$ erg sec^{-1} (Neuhäuser et al. 1999). The bolometric luminosity of this source is estimated at $\log(L_{\rm bol}/L_\odot) \approx -3.7$ (Schneider et al. 1991), giving

$\log(L_X/L_{\rm bol}) < -2.7$. The slow rotation and strong Hα activity place PC 0025 on the opposite end of the activity-rotation spectrum from BRI 0021 and LP 944-20.

2MASP J0345432+254023: This source is an isolated L0 dwarf, but it is still not clear whether it is a low mass star or a brown dwarf younger than ~ 1 Gyr (Kirkpatrick, Beichman & Skrutskie 1997). Leggett et al. (2001) estimate the luminosity of 2MASP J0345432+254023 (hereafter 2MASP 0345+25) at $\log(L_{\rm bol}/L_\odot) \approx -3.6$, with an effective temperature of 2000 K (see notes on TVLM 513 above). 2MASP 0345+25 has an upper limit on Hα emission of $\log(L_{\rm H\alpha}/L_{\rm bol}) \lesssim -5.6$.

2MASSW J0036159+182110: This source is a recently-discovered L3.5 candidate brown dwarf (Kirkpatrick et al. 2000; Gizis et al. 2000; Reid et al. 2000). 2MASSW J0036159+182110 (hereafter 2MASS 0036+18) shows no evidence of Li or Hα, with upper limits of EW$<$ 0.1A (Reid et al. 2000; Kirkpatrick et al. 2000). The temperature of 2MASS 0036+18 is estimated to be 1800 K based on the spectra and models of Leggett et al. (2001).

GD 165B: This source is a rapidly-rotating, $v\sin i \approx 37$ km sec^{-1}, L4 dwarf orbiting a white dwarf primary (Becklin & Zuckerman 1988). Kirkpatrick et al. (1999) used model atmospheres, including the effects of condensation and dust opacities, to estimate the temperature of this source, $T \approx 1900$ K, and in addition used the cooling age of the white dwarf primary to estimate the age of GD 165B at $1.2-5.5$ Gyr. Based on these two quantities they conclude that this source is likely a brown dwarf. The luminosity of GD 165B is estimated at $\log(L_{\rm bol}/L_\odot) \approx -4.1$ (Leggett et al. 2001). Along with DENIS-P J1228.2–1547 (see below), and possibly PC 0025, observations of GD 165B can be used to test the effect of binarity on radio emission from late dwarfs, and the 4" separation between the binary members allows us to pinpoint the source of any radio emission from the system.

2MASSW J1507476–162738: This source is a nearby L5 dwarf (Reid et al. 2000,2001). 2MASSW J1507476–162738 (hereafter 2MASS 1507–16) has only upper limits on Li and Hα of <0.1 A and <0.5 A, respectively (Kirkpatrick et al. 2000; Reid et al. 2000).

DENIS-P J1228.2–1547: This source is an L5 brown dwarf exhibiting relatively slow rotation, $v\sin i \approx 11$ km sec^{-1}, and no detectable Hα emission, $\log(L_{H\alpha}/L_{\rm bol}) \lesssim -5.3$ (Martín et al. 1997; Delfosse et al. 1997; Tinney, Delfosse & Forveille 1997). The bolometric luminosity of DENIS-P J1228.2–1547 (hereafter DENIS 1228) is estimated to be $\log(L_{\rm bol}/L_\odot) \approx -4$ to -4.3 (Leggett et al. 2001; Martín et al. 1997; Delfosse et al. 1997; Tinney, Delfosse & Forveille 1997), and its effective temperature is 1800 K (Leggett et al. 2001). In addition, DENIS 1228 has an upper limit on X-ray emission of $\log L_{\rm X} < 27.3$ erg sec^{-1}, and $\log(L_X/L_{\rm bol}) < -2.3$. Based on the detection of Li and the estimated effective temperature, the age and mass of DENIS 1228 are estimated to be M<0.065 M$_\odot$ and $t < 1$ Gyr (Tinney, Delfosse & Forveille 1997). Finally, Martín, Brandner & Basri (1999) have shown that DENIS 1228 is in fact a brown dwarf binary with a projected separation of approximately 5 AU. While our observations cannot resolve the system, we can study the combined emission, and effect of binarity on the production of this emission.

SDSS J134646.45-003150.4: This is the only methane (spectral class T6; Burgasser et al. 2001; Geballe et al. 2001) brown dwarf in the sample. It has a slightly higher effective temperature than that of two other known methane brown dwarfs, GL 229B and SDSS J162414.37+002915.6 (Tsvetanov et al. 2000), and it is inactive in Hα, with $\log(L_{\rm H\alpha}/L_{\rm bol}) \lesssim -5.3$ (Burgasser et al. 2000). The bolometric luminosity of SDSS J134646.45-003150.4 (hereafter SDSS 1346) is $\log(L_{\rm bol}/L_\odot) \approx -5.3$ (Burgasser et al. 2001; Tsvetanov et al. 2000). At a distance of only ~ 11 pc (Tsvetanov et al. 2000) SDSS 1346 is an excellent candidate for the detection of radio emission from this class of objects.

3. RADIO OBSERVATIONS

Very Large Array (VLA[1]) observations were conducted at 8.46 GHz in the standard continuum mode with 2×50 MHz contiguous bands. A log of all observations is given in Table 2. Following the detection of emission from BRI 0021 at 8.46 GHz, we also observed this source at 4.86 GHz. In all observations we used the extra-galactic sources 3C 48 (J0137+331) and 3C 286 (J1331+305) for flux calibration, while the phase was monitored using calibrator sources within $\sim 5^\circ$ of the survey sources.

The first set of observations was undertaken in the A and A$\rightarrow$B configurations. Unfortunately, half the data in these observations had to be discarded due to a malfunction of the lower Intermediate Frequency channel, and the resulting rms noise levels are therefore higher than the theoretical values by $\approx \sqrt{2}$. We repeated a subset of these observations over a period of approximately three weeks in the CnB configuration. The final set of observations, with five new targets was undertaken in the DnC configuration.

The data were reduced and analyzed using the Astronomical Image Processing System (AIPS, release 31DEC1999; Fomalont 1981). Both the visibility data and maps were inspected for data quality and noisy points were removed. To search for flares, we constructed lightcurves using the following method. We removed all the bright background sources in each image using the AIPS/IMAGR routine to CLEAN the region around each source, and the AIPS/UVSUB routine to subtract the resulting source models from the visibility data. We then plotted the real part of the complex visibilities at the position of each target source as a function of time using the AIPS/UVPLT routine. The background source subtraction is necessary since the side-lobes of these sources, and the change in the synthesized beam shape during the observation result in flux variations over the map, which may contaminate any real variability or generate false variability.

The uncertainties in the resulting lightcurves (Figures 1–4) are dominated by system thermal noise. The system temperature includes contribution from background sources, the sky, and hardware (e.g. receivers). At the observing frequency used in this survey, 8.46 GHz, the dominating term is the receiver noise. As a result, there are no significant systematic effects since in all cases the sources were located within a few arcseconds of the array pointing center, and the background source subtraction successfully removed possible contaminating sources. In fact, the plotted uncertainties, as well as the rms noise from the maps, are within a few percent of the theoretical

[1]The VLA is operated by the National Radio Astronomy Observatory, a facility of the National Science Foundation operated under cooperative agreement by Associated Universities, Inc.

noise estimates for the VLA at 8.46 GHz.

To further test the veracity of the resulting lightcurves and uncertainty estimates we constructed equivalent lightcurves for random positions on each map. We find that on average the fluctuations in these lightcurves do not exceed 2σ, and the noise estimates are similar.

4. RESULTS

We detected flares and persistent emission from TVLM 513, 2MASS 0036+18, and, with lower significance, from BRI 0021. Figures 1–4 show the lightcurves for observations of these sources. The peak flux densities range from ≈ 360 μJy in BRI 0021 to ≈ 980 μJy in TVLM 513, and the flare timescales (FWHM) range from ≈ 6 min in BRI 0021 to ≈ 20 min in 2MASS 0036+18. The resulting duty cycles, defined as the ratio of the time the sources produce flares to the total observing time, are $\approx 2-10\%$. In the case of BRI 0021, the value of 2% is consistent with a duty cycle of $\lesssim 7\%$ for Hα flares (Reid et al. 1999). The duty cycles of all three sources are consistent with an average Hα flare duty cycle of $\sim 7\%$ for late M dwarfs (Gizis et al. 2000).

The fraction of circular polarization during the flares is significant in TVLM 513, $f_{\rm circ} \approx 66 \pm 4\%$, and 2MASS 0036+18, $f_{\rm circ} \approx -62 \pm 5\%$, but is somewhat lower in BRI 0021, $f_{\rm circ} \approx 30 \pm 20\%$ (see Figures 1 and 3, and Table 3). The negative value for 2MASS 0036+18 indicates that the emission is left-handed circularly polarized.

In addition, we clearly detect persistent emission from TVLM 513 and 2MASS 0036+18, with flux densities of ≈ 190 μJy and ≈ 240 μJy, respectively. In the initial observation of 2MASS 0036+18 the persistent flux density was only ≈ 130 μJy. The detection of persistent emission from BRI 0021 is marginal, with an average value of 40 ± 13 μJy at 8.46 GHz from the combined observations is January and May. At 4.86 GHz the flux from this source is 40 ± 18 μJy, and it is not clear whether persistent emission is detected.

In addition to the change in persistent flux between the two observations of
2MASS 0036+18, the persistent emission from this source and TVLM 513 appears to vary within each observation. In the case of 2MASS 0036+18 the source brightened over the last 60 min of observation on Oct 9, possibly indicating a second strong flare (Figure 3). The sharp decrease in flux over the first 30 min of the observation could be the exponential tail of an earlier strong flare. An increase in flux was also observed towards the end of the observation from Sep 23 (Figure 2). In both cases, the rise time is similar to the observed flare from Oct 9, indicating that perhaps strong flares from this source are common, and have similar profiles.

It is therefore possible that the persistent emission is simply a superposition of several, possibly weaker, flares. If this is the case, the flare duty cycles for these two sources approach 100%. This is similar to LHS 2065, in which Martín & Ardila (2001) find that weak Hα flares may be more common than strong flares (see §2). The implications of such sustained flaring emission are discussed in §6.

We find no evidence for flares from the other nine sources. However, for most of the sources this is not surprising given the observed duty cycles of strong flares, and the required luminosities for a significant detection. The most luminous flare in the sample, from TVLM 513, can only be detected out to a distance of ≈ 20 pc with significance $\sim 5\sigma$. Five of the nine undetected sources lie at or beyond this distance. For the other four sources the flares could be weaker, undetected in the short observations (≈ 2 hr), or simply do not exist. Therefore, the lack of radio emission does not significantly constrain the production of flares in these sources, and the upper limits only provide constraints on the persistent emission.

The strong quiescent emission in TVLM 513 and 2MASS 0036+18 can only be detected out to a distance of ~ 15 pc in similar observations. Thus, some of the non-detections do not provide significant constraints given the detected luminosities. In Figures 5 and 6, and §6 we show that most of the upper limits on the ratio of radio luminosity to bolometric luminosity are consistent with the persistent luminosities of the detected sources. The most notable exception is the upper limit on emission from LHS 2065. We see from Figures 5 and 6 that the upper limit is comparable to the detection of quiescent emission from LP944-20 and the possible quiescent emission from BRI 0021. This non-detection also contrasts with the detection of Hα emission from this source (Martín & Ardila 2001). In addition, a comparison of the upper limits from Krishnamurthi, Leto & Linsky (1999) to the detections in this survey provides significant constraints on the lack of emission from their M7-M9 objects. As shown in Figures 5 and 6, their upper limits are up to an order of magnitude fainter in $L_{\rm rad}/L_{\rm bol}$ than the detected sources in this survey. We discuss the implications of these non-detections in detail in §6.

5. ANALYSIS OF THE RADIO EMISSION

To derive the properties of the flares and persistent emission, and the physical conditions that give rise to this radio emission, we model the lightcurves of TVLM 513 and BRI 0021 with a Gaussian profile:

$$F_\nu(t) = F_{\nu,{\rm q}} + F_{\nu,0} \exp\left[-\frac{1}{2}\left(\frac{t-t_0}{\sigma_{\rm t}}\right)^2\right]. \quad (1)$$

Here, $F_{\nu,{\rm q}}$ is the quiescent component, t_0 is the flare peak time relative to the start of the observation, $\sigma_{\rm t}$ is the HWHM duration of the flare, $F_{\nu,0}$ is the peak flux, and we absorbed the normalization factor of $1/\sqrt{2\pi\sigma_{\rm t}^2}$ into the definition of $F_{\nu,0}$. The lightcurve of 2MASS 0036+18 from Oct 9 is not well-described by this model, and we instead use an exponential profile, in which the Gaussian in Equation 1 is replaced by rising and decaying exponentials with timescales $\tau_{\rm r}$ and $\tau_{\rm d}$, respectively (Figure 3). In Table 3 we summarize the derived parameters for each source. We note that the profile of the flare from 2MASS 0036+18 is somewhat unusual since flares usually exhibit a rapid rise and exponential decay as opposed to the slow rise and fast decay in this case (Figure 3). A similar profile was found for two of the three flares from LP 944-20 (B01).

The fits to the lightcurves of TVLM 513 (Figure 1) and 2MASS 0036+18 (Figure 3), have unsatisfactory χ^2 values, ~ 3 per degree of freedom. This is due to significant variability in the persistent component, indicating that it is possibly a superposition of multiple flares, rather than a truly constant component.

The statistical significance of the flare detections are determined by the level at which we can rule out the hypothesis that $F_{\nu,0} = 0$ in Equation 1, coupled with the number of time bins in each lightcurve. For the flares from TVLM 513 and

2MASS 0036+18 the detections are secure, with significance levels of $\sim 20\sigma$. The flare from BRI 0021 has a lower statistical significance of 4.5σ, but this is still high enough for a significant detection. We further tested the significance of this flare by constructing equivalent lightcurves for random positions on the map. We find an average fluctuation of 2σ, and no fluctuations larger than 2.5σ, indicating that the increase in flux in BRI 0021 is a likely flare.

It is important to note that even if the short-timescale increase in flux in the BRI 0021 lightcurve is simply a 4.5σ statistical fluctuation in the lightcurve, the flux density of this source from the combined observations on Jan 25 and May 21 is 83 ± 15 μJy, and hence significant at the 5.5σ level. Therefore, whether this detection is of persistent emission or a faint flare, this source is radio active.

The peak-flare luminosities are in the range $L_{\nu,\rm f} \approx (6-13) \times 10^{13}$ erg sec^{-1} Hz^{-1}, more luminous than the brightest Solar flares, $L_{\nu,\rm f} \approx 2 \times 10^{12}$ erg sec^{-1} Hz^{-1} (Bastian, Benz & Gary 1998), but somewhat weaker than flares from active early M dwarfs (e.g. White, Jackson & Kundu 1989). The ratio of flaring radio to bolometric luminosity is higher by a factor of $\sim 10^5$ than for Solar flares, but is very similar to flares on early M dwarfs (see Figures 5 and 6) since the lower luminosity of the flares relative to those from early M dwarfs is compensated by the lower bolometric luminosity of the late M and L dwarfs in this sample. The persistent luminosities are lower by factors of 3, 5, and 9 than the flare luminosities in 2MASS 0036+18, TVLM 513, and BRI 0021, respectively.

The radio band energy release in the flares is $E_R \sim 1.4 \times 10^{23} d_{\rm pc}^2 \nu_{\rm GHz} F_{\nu,\rm mJy} \sigma_{t,\rm min} \approx (2-10) \times 10^{26}$ erg, with the lowest energy release in the flare from BRI 0021, and the highest in the flare from TVLM 513. In making this estimate we have assumed that the flare spectral energy distribution peaks near 8.5 GHz, and has steep spectral slopes below and above this frequency, so that the bulk of the energy release is at ~ 8.5 GHz. This assumption is justified since for synchrotron emission (see §5.2) the spectral slope below the peak (self-absorbed portion) is $F_\nu \propto \nu^{2.5}$, while above the peak typical values ranges from $\sim \nu^{-1.5}$ to ν^{-4} (e.g. Dulk & Marsh 1982). The high fraction of circular polarization in the two bright flares from TVLM 513 and 2MASP 0345+25 indicates that the observing frequency (8.46 GHz) lies at or above the peak frequency, while observations of flares from several early M dwarfs (Leto et al. 2000) show that in these sources the flux drops significantly above 8.5 GHz. In fact, for the M5.5 dwarf UV Cet the spectral slope above 8.5 GHz is constrained to be lower than –2.3. Therefore, it is likely that most of the energy in the observed flares in this survey is released at 8.5 GHz.

5.1. *Violation of the Guedel–Benz relations*

One of the puzzling facts about the radio emission from LP 944-20 (B01) is that despite its spectral type (M9) it violates the Guedel–Benz relations (which hold for spectral types <M7) by four orders of magnitude. Here we examine whether any of the sources detected in this survey show a similar violation of these relations.

Based on these relations, and the flare duty cycle we find that the expected X-ray luminosity of BRI 0021 is $L_{\rm X,pred} \approx 2.6 \times 10^{28}$ erg sec^{-1}, dominated by the persistent component. This value is $\gtrsim 10^3$ times larger than an upper limit of $L_{\rm X} < 2.6 \times 10^{25}$ erg sec^{-1} from a 63.2 ksec ROSAT observation (Neuhäuser et al. 1999). Even if we neglect the persistent emission, the predicted luminosity due to flares is a factor of > 150 too high. Finally, if the observed increase in the radio flux is a statistical fluctuation rather than a genuine flare, and the flux of the source is steady at 83 ± 15 μJy, this emission violates the Guedel–Benz relations by a factor of > 1700. Therefore, regardless of whether the radio emission from this source is flaring or persistent (or both), it violates the Guedel–Benz relations by several orders of magnitude. This is puzzling since, as in the case of LP 944-20, BRI 0021 has spectral type M9.5, indicating that radio and X-ray emission become uncorrelated over a narrow range of spectral type.

As far as we know, TVLM 513 and 2MASS 0036+18 have not been observed in X-rays, so a similar analysis is not possible. However, we can still show that the radio emission from these sources is much stronger relative to the bolometric luminosity than in early-mid M dwarfs, based on a comparison of the predicted peak X-ray luminosity and the bolometric luminosity. In the case of TVLM 513, the predicted peak X-ray luminosity is $\approx 4 \times 10^{29}$ erg sec^{-1}, which is approximately 25% of the bolometric luminosity of this source. In 2MASS 0036+18 this ratio is even higher, $\sim 50\%$. Liebert et al. (1999), among others, have found a similar result for Hα flares, and noted that these flares may release more energy relative to the bolometric luminosity than in earlier spectral types.

Therefore, while the Guedel–Benz relations hold for spectral types <M7, there is some indication from LP 944-20 and BRI 0021 that these relations break down around spectral type M9. This possibly indicates a sudden change in the mechanism that gives rise to the radio emission. We note that radio and X-ray observations of a larger sample are required to test this idea comprehensively.

5.2. *Magnetic Fields and Coronal Densities*

So far, we have analyzed the radio emission in a relatively model-independent way. However, the next step is to determine the emission mechanism and physical conditions that gave rise to the flares and persistent emission. The first step in this analysis is to calculate the brightness temperatures:

$$T_{\rm b} \approx 2 \times 10^9 F_{\nu,\rm mJy} d_{\rm pc}^2 \nu_{\rm GHz}^{-2} (R/R_{\rm J})^{-2}. \quad (2)$$

Assuming that the emission is coronal, we can use $R \sim (2-4) R_{\rm s} \sim (2-4)\, R_{\rm J}$ as the size of the corona in units of Jupiter radii (Linsky & Gary 1983; Dorman, Nelson, & Chau 1989; Burrows, Hubbard, & Lunine 1989; Chabrier et al. 2000; Leto et al. 2000). These size estimates lead to brightness temperatures of $\approx 10^8 - 10^9$ K during the flares, and $\approx 10^7 - 10^8$ K for the persistent emission. Alternatively, it is possible that the flares arise from much smaller regions (e.g. coronal loops), in which case the brightness temperatures would exceed 10^{11} K, if $R_{\rm loop} \sim 0.1 R_{\rm s} \sim 0.1 R_{\rm J}$. While we have no data to constrain the size of the coronae in these sources, it is likely that the actual brightness temperatures are within the range defined by these estimates.

The high brightness temperatures indicate that the emission is non-thermal. Most likely it arises from the incoherent gyrosynchrotron or synchrotron processes (Dulk & Marsh 1982; Dulk 1985), but coherent emission is also applicable if the flares actually have $T_{\rm b} \sim 10^{11}$ K. The high degree of circular polariza-

tion in the flares from TVLM 513 and 2MASS 0036+18 possibly favors coherent emission, but can also be achieved in gyrosynchrotron emission (Dulk 1987). On the other hand, the high frequency of the observed emission, $\nu = 8.46$ GHz, favors incoherent emission since coherent emission is limited to $\lesssim 10$ GHz (Bastian, Benz & Gary 1998; Stepanov et al. 2001). Since it is not clear which emission process produces the observed radio emission, we estimate the magnetic field strengths and coronal densities using both.

To accurately calculate the magnetic field strengths and coronal densities in the radio active sources using the gyrosynchrotron formulation, requires detailed spectral and geometrical information, since the results depend sensitively on the high-frequency spectral slope, the viewing angle, and the geometry of the emission region (Dulk & Marsh 1982; Dulk 1985). For approximate values we can instead use the synchrotron formulation, along with the approximation $f_{\rm circ} \approx 3/\gamma_{\rm min}$, where $\gamma_{\rm min}$ is the minimum Lorentz factor of the radio-emitting electron distribution. For TVLM 513 and 2MASS 0036+18, the Lorentz factor is $\gamma_{\rm min} \approx 5$, while for BRI 0021 it is $\gamma_{\rm min} \sim 10$. The resulting magnetic field strengths are $B \approx 57 \nu_{\rm m,GHz} \gamma_{\rm min}^{-2} \approx 20$ G in TVLM 513 and 2MASS 0036+18, and ≈ 5 G in BRI 0021. These values should be treated with caution, and they can vary upward by an order of magnitude or more. In fact, if we choose characteristic values for the radio spectral index and the viewing angle, we find gyrosynchrotron values of $B \sim 350$ G for TVLM 513 and 2MASS 0036+18, and $B \sim 50$ G for BRI 0021.

For comparison, the Solar magnetic field as inferred from a multi-wavelength study of three Solar flares (Kundu et al. 2001) ranges from $300-900$ G at the loop footpoints, while fields in active early M dwarfs reach strengths of a few kG (Saar & Linsky 1985; Haisch, Strong & Rodono 1991; Johns-Krull & Valenti 1996; Stepanov et al. 2001).

The total number of electrons in the synchrotron formulation is easily calculated using $N_{\rm e} \approx 10^{36} d_{\rm pc}^2 F_{\nu a,{\rm mJy}} \gamma_{\rm min}^{-2} B_{\rm min}^{-2} \approx (5-20) \times 10^{33}$. However, to calculate the densities we have to know the geometry of the flare region. In the gyrosynchrotron formulation, using the magnetic field values quoted above, we find column densities of $\sim 10^{19}$ cm^{-2} for TVLM 513 and 2MASS 0036+18, and $\sim 10^{22}$ cm^{-2} for BRI 0021. These densities are similar to those calculated for Solar and M dwarf flares (Bruggmann & Magun 1990; Stepanov et al. 2001).

Alternatively, if the flare brightness temperatures are of the order of 10^{11} K, then we must use coherent emission to estimate the magnetic field strengths and the densities. There are two main coherent processes, electron cyclotron maser (ECM), and plasma emission, which operate at the fundamental frequencies $\nu_c \approx 2.8B$ MHz and $\nu_p \approx 9n^{1/2}$ kHz, respectively. Recently, Stepanov et al. (2001) have shown for the flare star AD Leonis that emission due to the ECM process is strongly damped by thermal electrons in the corona. They conclude that for typical coronal temperatures and densities plasma emission is the more likely process.

Plasma radiation is primarily emitted at $\nu \approx \nu_p$. Thus, we can simply use $\nu_p \sim 8.5$ GHz to find $n \sim 10^{12}$ cm^{-3}, and approximate $\nu_c \lesssim 0.5\nu_p$ to find $B \lesssim 1500$ G. These values are consistent with the gyrosynchrotron-derived values. Therefore, we conclude that regardless of the exact emission mechanism or magnetic field configuration, the observations are consistent with magnetic fields in the range $10-10^3$ G, and coronal densities of the order of 10^{12} cm^{-3}. We discuss the implications of the inferred magnetic field values and coronal densities in more detail in §6.

5.3. *Heating Mechanisms*

We next investigate whether our radio data support a particular model of coronal particle acceleration. Heating can be due to acoustic waves generated by the same turbulent convection that presumably gives rise to the magnetic fields (Bohn 1984; Ulmschneider, Theurer, & Musielak 1996). Ulmschneider et al. (1996) provide an estimate of the total flux due to acoustic heating, $F_{\rm A}$, as a function of effective temperature and surface gravity based on an extended Kolmogorov turbulent energy spectrum. We use their Table 1 to estimate $\log(L_{\rm A}/L_{\rm bol}) \sim -13$ for our survey sources. In comparison, the values for the observed radio flares are $\log(L_{\rm rad,f}/L_{\rm bol}) \sim -6$ (Figures 5 and 6). Therefore acoustic heating cannot supply the necessary energy to power the flares, and similarly, cannot explain the persistent emission with $\log(L_{\rm rad,q}/L_{\rm bol}) \sim -7$.

A more plausible heating mechanism is magnetic reconnection (Bastian, Benz & Gary 1998; Sturrock 1999). This model can also explain the persistent emission if it is a superposition of weaker flares. In the context of this model, the flares are produced when coronal magnetic loops reconnect, release energy, and create a current sheet along which ambient electrons are accelerated. Recent work on three-dimensional reconnection shows that the particles are accelerated into a power-law energy distribution (Schopper, Birk & Lesch 1999), as required for the synchrotron and gyrosynchrotron discussion in §5.2. The accelerated electrons drive an outflow of hot plasma into the corona as they interact with, and heat chromospheric material (i.e. chromospheric evaporation). The interaction of the outflowing plasma with the same electons produces X-ray emission via the bremsstrahlung process (Neupert 1968; Hawley et al. 1995; Guedel et al. 1996). This so-called Neupert effect indicates that there is a *causal* connection between particle acceleration, which is the source of radio emission, and plasma heating, which results in X-ray emission. This connection explains the phenomenological Guedel–Benz relations.

It is possible that the violation of the Guedel–Benz relations in the emission from LP 944-20 and BRI 0021 indicates that the Neupert effect no longer holds in late M dwarfs. A direct test of this possibility requires simultaneous observations of such sources in the radio and X-rays. Future surveys of activity in late M and L dwarfs would be considerably more effective if they followed such a strategy.

It is also possible that the energy source for the radio emission in the active survey sources and LP 944-20 is an altogether different process, in which case a causal relation between radio emission and activity in other bands would not be required. At present it is not possible to distinguish between these different possibilities, but future observations with wide spectral coverage will likely provide an answer.

6. DISCUSSION

Before we proceed to interpret the results of this survey in the context of correlations between radio activity and physical source parameters, we summarize the main observational results: (i) the observed flares have approximately equal luminosity, ratio of radio to bolometric luminosity, and released energy, (ii) the persistent emission has approximately the same

luminosity, and it appears to be variable, (iii) LHS 2065 has an upper limit on the ratio of radio to bolometric luminosity which is lower than the detected persistent emission, despite being active in Hα, (iv) the emission from BRI 0021, as well as LP 944-20, violates the Guedel–Benz relations by several orders of magnitude, (v) the inferred magnetic field strengths are $\sim 10-10^3$ G, and the coronal densities are $\sim 10^{12}$ cm^{-3}, and (vi) the heating mechanism is probably magnetic reconnection, but it is possible that the Neupert effect is violated.

A comparison of these results to the radio properties of LP 944-20 (B01) is illustrative. The peak luminosity of the flares from all four sources varies by only a factor of two, and the energy release only varies by a factor of five. The ratio of the flare peak luminosity to the bolometric luminosity of each source is $\log(L_{\rm rad,f}/L_{\rm bol}) \approx -6$, and the ratio for the quiescent luminosities is $\log(L_{\rm rad,q}/L_{\rm bol}) \approx -7.5$ to -6.5 (Figures 5 and 6).

We find similar results when we compare this sample to other M dwarfs that have been observed in the radio. For example, flares have been detected from the dM3.5e dwarf Ad Leo (Stepanov et al. 2001), the dM4e dwarf Rst 137B (Lim 1993), and the dM5.5e dwarf Proxima Centauri (Lim, White & Slee 1996), with ratios of $L_{\rm rad}/L_{\rm bol}$ that are in the range of ~ -6 to -8. These values are plotted in Figures 5 and 6a, and we can see that with the exception of the flare from Proxima Centauri, which is fainter by approximately two orders of magnitude, these values are similar to those observed in this survey and in LP 944-20. The flat distribution of $L_{\rm rad}/L_{\rm bol}$ for the flares from the sources with spectral types M8-L3.5, and perhaps M3.5-L3.5 (with the exception of Proxima Centauri), possibly points to a "saturation" effect, in which $L_{\rm rad,f}/L_{\rm bol}$ reaches a maximum value that is independent of spectral type or other physical properties. It is beyond the scope of this paper and data to assess this possibility in detail.

The pattern of persistent radio emission in early M dwarfs through L dwarfs is more puzzling. In Figures 5 and 6b we plot the ratios of persistent radio to bolometric luminosities for the detections and upper limits in this survey, the upper limits from Krishnamurthi, Leto & Linsky (1999), and detections in the range M3-M6.5 (Cash, Charles & Johnson 1980; Pallavicini, Wilosn & Lang 1985; Leto et al. 2000). Despite the small sample, there is a clear increase in the ratio of persistent radio to bolometric luminosity over the range M3-L3.5 (dashed and dotted lines in Figure 6b). This increase is in direct contradiction with the steep decline in Hα activity beyond spectral type M7 (Gizis et al. 2000). In fact, while the Hα activity drops by approximately 1.5 orders of magnitude between M7 and L3.5, the radio activity appears to *increase* by a similar amount in the same spectral range. This indicates that the radio and Hα activity are probably not correlated at the bottom of the main sequence.

Another interesting result from Figure 6b is that there are several upper limits, which appear to fall below the apparent steady increase in $L_{\rm rad}/L_{\rm bol}$. These upper limits are for 2MASS 1507–16 (L5) and SDSS 1346 (T6) from this survey, and five sources from Krishnamurthi, Leto & Linsky (1999): VB 8 (M7), VB 10 (M8), GL 569B (M8.5), LHS 2065 (M9), and Gl 229B (T); we use the upper limit for LHS 2065 from Krishnamurthi, Leto & Linsky (1999) since it is approximately 3 times lower than the value measured in our survey. While some variance in activity levels within the sample of M and L dwarfs is not unexpected, it is interesting to investigate whether these source have some property which differentiates them from the detected sources. In Figure 7 we plot the ratio of persistent radio to bolometric luminosity as a function of the source rotational velocity, and we find that of these seven sources the three with measured rotational velocities have $v\sin i < 10$ km sec^{-1}, while the detected sources have $v\sin i > 30$ km sec^{-1}. In fact, the source with the most constraining upper limit (VB 8) has the lowest rotational velocity in the sample, while the source with the highest value of $L_{\rm rad}/L_{\rm bol}$ (TVLM 513) has the highest rotational velocity. The upper limit on the radio activity from the fast rotator Kelu 1 (Krishnamurthi, Leto & Linsky 1999), with $v\sin i \approx 60$ km sec^{-1} (Basri et al. 2000) is three times higher than the detected fast rotators, and therefore does not constrain the possible relation between radio activity and rotational velocity.

We note that while these sources provide tantalizing evidence for a relation between rapid rotation and radio activity, the sample is still very small. Future observations of a larger sample will provide a better test of this possible relation. However, it is already possible to rule out the idea that high rotational velocities quench the magnetic dynamo through supersaturation (Randich 1998), as was inferred from the drop in persistent Hα and X-ray activity in late M and L dwarfs.

The most puzzling implication of the observed radio emission, regardless of its possible correlation with fast rotation, is that late M and L dwarfs posses appreciable and sustained magnetic fields, as well as high particle densities in at least some regions of their coronae. This result seems to contradict recent calculations by Mohanty et al. (2002) which indicate that the generation and propagation of magnetic energy decreases with decreasing effective temperature, resulting in a decrease of coronal activity in late spectral types.

In addition, the presence of magnetic fields and ionized material indicates that magnetic braking should have slowed these sources down considerably. Thus, it is not clear how these sources maintain such high rotational velocities.

No other correlations are apparent from the data. For example, the upper limit on the young object CRBR 15 is approximately five times higher than the faintest detected persistent emission, and therefore precludes any conclusion on the role of age in the production of radio emission. Similarly, the upper limits on emission from the confirmed binary systems DENIS 1228 and GD 165B are approximately forty times higher than the detected sources, and it is therefore not possible to assess the role of binary interaction in the production of radio emission.

7. CONCLUSIONS

We detected flaring and persistent emission at 8.46 GHz from the M and L dwarfs TVLM 513, 2MASS 0036+18, and BRI 0021, but no emission from the nine other survey sources. These observations lead to several interesting conclusions, which are puzzling given the decrease in persistent Hα and X-ray activity in late M and L dwarfs.

The flares and persistent emission from the three survey sources, as well as LP 944-20 (B01) have similar properties. In particular, the emission from these sources has similar $L_{\rm rad}/L_{\rm bol}$ values, and energy release. This probably points to a common emission mechanism and physical conditions (e.g. magnetic fields) in these sources.

In addition, while the dependence of Hα activity on rota-

tion appears to break down in early-mid M dwarfs, the radio active sources for which the rotational velocity is known are rapid rotators, with the most luminous source in the sample, TVLM 513, having the highest rotational velocity, $v\sin i \approx 60$ km sec^{-1}. At the same time, the limits on radio activity in three slow rotators from Krishnamurthi, Leto & Linsky (1999) indicate that they are less active than the detected sources in this sample, pointing to a possible relation between rotation and radio activity. Regardless of whether a correlation actually exists, the radio emission requires magnetic fields and coronal densities that should have resulted in significant slow-down due to magnetic braking. It is still not clear how these sources maintain their rapid rotation.

Possibly related to the differences in radio activity and other activity indicators is the violation of the Guedel–Benz relations in BRI 0021 and LP 944-20. In these two sources, the predicted X-ray emission is over-luminous relative to X-ray observations. This indicates that radio and X-ray activity are no longer correlated in some late M dwarfs, in the same way that radio and Hα activity appear to be uncorrelated. Moreover, it appears that the breakdown in the Guedel–Benz relations occurs over a narrow spectral type range, M7-M9.

The observed persistent emission is clearly variable, possibly on a timescale of the order of one hour (Figures 1 and 3). It is possible that this emission is simply a superposition of weak flares, in which case the activity duty cycle is $\sim 100\%$. However, if this component is truly persistent over long timescales, it means that our understanding of magnetic field generation in very low mass stars is far from complete. Longer, multi-frequency observations are required for a thorough understanding of the origin of this emission component.

To address the possible correlation between rotation and radio activity, as well as the differences between the activity indicators (i.e. radio, Hα, and X-rays), and to gain a deeper understanding of physical processes in dwarf stars it is necessary to carry out a comprehensive, multi-wavelength survey of nearby M and L dwarfs. In particular, it is crucial to observe a wide variety of objects for each spectral type, and to reach ratios of $\log(L_{\rm rad}/L_{\rm bol}) < -8$. Despite the complexity of such an effort, the results will impact a wide range of fields from dynamo theory to the formation of brown dwarfs.

I thank B. Clarke for re-scheduling some of the VLA time awarded to this project. I also thank R. Rutledge, D. Frail, S. Kulkarni, and D. Reichart for valuable discussions, and the anonymous referee for many helpful comments and suggestions. This research has made use of the Online Brown Dwarf Catalog (http://ganymede.nmsu.edu/crom/cat.html), which is compiled and maintained by Christopher R. Gelino at New Mexico State University, the SIMBAD database operated at CDS, Strasbourg, France, and NASA's Astrophysics Data System Abstract Service

REFERENCES

Basri, G. & Marcy, G. W. 1995, AJ, 109, 762.
Basri, G., et al. 2000, ApJ, 538, 363.
Bastian, T. S., Benz, A. O., & Gary, D. E. 1998, ARAA, 36, 131.
Becklin, E. E. & Zuckerman, B. 1988, Nature, 336, 656.
Benz, A. O. & Guedel, M. 1994, A&A, 285, 621.
Berger, E. et al. 2001, Nature, 410, 338.
Bessell, M. S. 1991, AJ, 101, 662.
Bohn, H. U. 1984, A&A, 136, 338.
Bruggmann, G., & Magun, A. 1990, A&A, 239, 347.
Burgasser, A. J., et al. 2000, AJ, 120, 473.
Burgasser, A. J., et al. 2001, accepted to ApJ; astro-ph/0108452.
Burrows, A., Hubbard, W. B., & Lunine, J. I. 1989, ApJ, 345, 939.
Burrows, A., et al. 1997, ApJ, 491, 856.
Cash, W., Charles, P., & Johnson, H. M. 1980, ApJ, 239, 23.
Chabrier, G., et al. 2000, ApJ, 542, 464.
Delfosse, X., et al. 1997, A&A, 327, L25.
Dorman, B., Nelson, L. A., & Chau, W. Y. 1989, ApJ, 342, 1003.
Dulk, G. A., & Marsh, K. A. 1982, ApJ, 259, 350.
Dulk, G. A. 1985, ARAA, 23, 169.
Dulk, G. A. 1987, *Cool Stars, Stellar Systems, and the Sun. Fifth Cambridge Workshop*, Linsky, J. L. & Stencel, R. E. eds. Springer-Verlag (Berlin).
Durney, B. R., De Young, D. S., & Roxburgh, I. W. 1993, Sol. Phys., 145, 207.
Fomalont, E. 1981, NRAO Newslett, 3, 3.
Geballe, T. R., et al. 2001, accepted to ApJ; astro-ph/0108443.
Gizis, J. E., et al. 2000, AJ, 120, 1085.
Graham, J. R., et al. 1992, AJ, 104, 2016.
Guedel, M. & Benz, A. O. 1993, ApJ, 405, L63.
Guedel, M., et al. 1996, ApJ, 471, 1002.
Haisch, B., Strong, K. T., & Rodono, M. 1991, ARAA, 29, 275.
Hawley, S. L., et al. 1995, ApJ, 453, 464.
Hawley, S. L., Gizis, J. E., & Reid, I. N. 1996, AJ, 112, 2799.
Imanishi, K., Tsujimoto, M., & Koyama, K. 2001, ApJ, 563, 361.
Johns-Krull, C. M., & Valenti, J. A. 1996, ApJ, 459, L95.
Kirkpatrick, J. D., et al. 1993, ApJ, 402, 643.
Kirkpatrick, J. D., Beichman, C. A., & Skrutskie, M. F. 1997, ApJ, 476, 311.
Kirkpatrick, J. D., et al. 1999, ApJ, 519, 834.
Kirkpatrick, J. D., et al. 2000, AJ, 120, 447.
Krishnamurthi, A., Leto, G., & Linsky, J. L. 1999, AJ, 118, 1369.
Kundu, M. R., et al. 2001, ApJ, 557, 880.
Legget, S. K., Allard, F., & Hauschildt, P. H. 1998, ApJ, 509, 836.
Leggett, S. K., et al. 2001, ApJ, 548, 908.
Leto, G., et al. 2000, A&A, 359, 1035.
Liebert, J., et al. 1999, ApJ, 519, 345.
Lim, J. 1993, ApJ, 405, L33.
Lim, J., White, S. M., & Slee, O. B. 1996, ApJ, 460, 976.
Linsky, J. L., & Gary, D. E. 1983, ApJ, 274, 776.
Luhman, K. L., & Rieke, G. H. 1999, ApJ, 525, 440.
Martín, E. L., Rebolo, R., & Magazzu, A. 1994, ApJ, 436, 262.
Martín, E. L., et al. 1997, A&A, 327, L29.
Martín, E. L., Basri, G., & Zapatero Osorio, M. R. 1999, AJ, 118, 1005.
Martín, E. L., et al. 1999, AJ, 118, 2466.
Martín, E. L., Brandner, W., & Basri, G. 1999, Science, 283, 1718.
Martín, E. L., & Ardila, D. R. 2001, AJ, 121, 2758.
Mohanty, S., et al. 2002, Accepted to ApJ; astro-ph/0201518.
Motte, F., Andre, P., & Neri, R. 1998, A&A, 336, 150.
Mould, J., Cohen, J., Oke, J. B., & Reid, N. 1994, AJ, 107, 2222.
Neuhäuser, R., it et al. 1999, A&A, 343, 883.
Neupert, W. M. 1968, ApJ, 153, L59.
Pallavicini, R., Willson, R. F., & Lang, K. R. 1985, A&A, 149, 95.
Randich, S. 1998, *Cool Stars, Stellar Systems, and the Sun. Tenth Cambridge Workshop*, Donahue, R. A. & Bookbinder, J. A. eds. ASP Conf Ser 154 (San Francisco), CD-1819.
Reid, I. N., et al. 1999, ApJ, 527, L105.
Reid, I. N., et al. 2000, AJ, 119, 369.
Reid, I. N., et al. 2001, AJ, 121, 1710.
Rutledge, R. E., et al. 2000, ApJ, 538, L141.
Saar, S. H., & Linsky, J. L. 1985, ApJ, 299, L47.
Schneider, D. P., et al. 1991, AJ, 102, 1180.
Schopper, R., Birk, G. T., & Lesch, H. 1999, Phys. of Plasmas, 6, 4318; astro-ph/0106561.
Stepanov, A. V., et al. 2001, A&A, 374, 1072.
Sturrock, P. A. 1999, ApJ, 521, 451.
Tinney, C. G. 1993, ApJ, 414, 279.
Tinney, C. G., et al. 1995, AJ, 110, 3014.
Tinney, C. G., Delfosse, X., & Forveille, T. 1997, ApJ, 490, L95.
Tinney, C. G. & Reid, I. N. 1998, MNRAS, 301, 1031.
Tsvetanov, Z. I., et al. 2000, ApJ, 531, L61.
Ulmschneider, P., Theurer, J., & Musielak, Z. E. 1996, A&A, 315, 212.
White, S. M., Jackson, P. D., & Kundu, M. R. 1989, ApJS, 71, 895.
Wilking, B. A., Greene, T. P., & Meyer, M. R. 1999, AJ, 117, 469.

TABLE 1
PROPERTIES OF THE SURVEY SOURCES

Source	Spect. Type.	Dist. (pc)	$T_{\rm eff}$ (K)	Age (Myr)	$v\sin i$ (km/sec)	Log($L_{\rm bol}/L_{\odot}$)	Log($L_{\rm H\alpha}/L_{\rm bol}$)	Log(L_X) (erg/sec)	Pred. $F_{\nu,R}$ (μJy)	Flares?
CRBR 15	M5	160	2930	< 3		–1.3		< 28.0	< 0.1	no
LHS 2243	M8	17	2880		< 5		–3.6			yes
TVLM 513	M8.5	10.5	2500/2880		60	–3.6				no
LHS 2065	M9	8.5	2100/2630	> 500	9	–3.5	–4	26.6	1.5	yes
BRI 0021	M9.5	12	2300		42 ± 8	–3.5	–6.3	< 25.4	< 0.05	yes
PC 0025	M9.5	62	2000	< 1000	13 ± 3	–3.7	–3.4	< 27.2	0.2	no
2MASP 0345+25	L0	27	2000	< 1000		–3.6	< -5.6			no
2MASS 0036+18	L3.5	9	1800	> 1000						no
GD 165B	L4	32	1900	< 1200	38	–4.0	< -5.2			no
2MASS 1507–16	L5	8	1700	> 1000						no
DENIS 1228	L5	20	< 1800	< 1000	11	–4.3	< -5.3	< 27.3	< 3	no
SDSS 1346	T6	11	~ 900			–5.3	< -5.3			no
LP 944-20	M9	5	2200	~ 550	30	–3.8	–5	25.7	0.5	yes

NOTE.—List of objects observed in this survey; LP 944-20 is included for completeness. The columns are (left to right), (1) source name, (2) spectral type, (3) distance, (4) effective temperature, (5) approximate age, (6) rotational velocity, (7) bolometric luminosity, (8) ratio of Hα luminosity to bolometric luminosity; for PC 0025+0447 the Hα emission is persistent, while for LHS 2243, LHS 2065, BRI 0021, and LP 944-20 it is flaring, (9) X-ray luminosity; for LP 944-20 this is the peak-flare luminosity (Rutledge et al. 2000), (10) predicted radio flux densities based on the X-ray luminosities and the Guedel–Benz relations (Guedel & Benz 1993; Benz & Guedel 1994); these values are for 5 GHz and should be higher at most by a factor of four for the observing frequency in this survey, ν = 8.46 GHz, and (11) indicates whether Hα or X-ray flares have been detected from the source. A more detailed description of the sources, and the relevant references are given in §2

TABLE 2
VERY LARGE ARRAY OBSERVATIONS

Source	Date (UT)	Array Config.	beam size (arcsec)	$t^{\rm on-source}$ (ksec)	ν_0 (GHz)	S$\pm\sigma$ (μJy)
PC 0025+0447	2001 Jan 25.85	A	0.34×0.24	3.7	8.46	< 137
BRI 0021−0214	2001 Jan 25.93	A	0.33×0.26	5.0	8.46	84 ± 27
2MASP J0345432+254023	2001 Jan 26.01	A	0.30×0.26	5.0	8.46	< 125
DENIS-P J1228.2−1547	2001 Jan 29.34	A→B	0.78×0.56	4.9	8.46	< 154
SDSS J134646.45-003150.4	2001 Jan 30.43	A→B	0.65×0.37	5.3	8.46	< 106
GD 165B	2001 Jan 30.51	A→B	0.64×0.31	5.3	8.46	< 97
CRBR 15	2001 Jan 30.60	A→B	0.72×0.48	4.5	8.46	< 149
DENIS-P J1228.2−1547	2001 May 29.20	CnB	1.6×0.86	4.3	8.46	< 87
BRI 0021−0214	2001 May 21.54	CnB	4.4×2.9	5.5	8.46	83 ± 18
BRI 0021−0214	2001 June 11.46	CnB	4.6×4.1	6.4	4.86	< 94
2MASP J0345432+254023	2001 June 11.58	CnB	3.0×1.7	5.1	8.46	< 88
SDSS J134646.45-003150.4	2001 June 20.24	CnB	4.7×1.9	5.1	8.46	< 68
PC 0025+0447	2001 June 20.41	CnB	4.8×1.8	5.0	8.46	< 75
2MASSW J0036159+182110	2001 Sep 23.44	DnC	12.1×8.2	7.8	8.46	135 ± 14
LHS 2065	2001 Sep 23.55	DnC	12.5×7.5	6.6	8.46	< 81
LHS 2243	2001 Sep 23.64	DnC	8.8×7.7	6.6	8.46	< 76
TVLM 513-46546	2001 Sep 23.73	DnC	11.5×9.8	6.6	8.46	308 ± 16
2MASSW J1507476−162738	2001 Sep 23.81	DnC	12.3×7.9	7.8	8.46	< 58
2MASSW J0036159+182110	2001 Oct 9.13	DnC	11.2×7.8	9.6	8.46	327 ± 14
LHS 2065	2001 Oct 12.66	D	11.2×7.8	3.6	8.46	< 95
LHS 2243	2001 Nov 1.42	D	10.2×9.2	11.1	8.46	< 47

NOTE.—The columns are (left to right), (1) Source name, (2) UT date of the start of each observation, (3) array configuration, (4) synthesized beam size, (5) total on-source observing time, (6) observing frequency, and (7) peak flux density at the position of each source, with the error given as the rms noise in the image; upper limits are the flux at the position of the source plus 3σ.

TABLE 3
PROPERTIES OF THE RADIO EMISSION

Parameter	TVLM 513	2MASS 0036+18 (Sep 23.44)	2MASS 0036+18 (Oct 9.13)	BRI 0021 (May 21.54)
Ave. Flux (μJy)	308 ± 16	135 ± 14	327 ± 14	83 ± 18
Ave. $f_{\rm circ}$ (%)	46 ± 4	-46 ± 11	-43 ± 3	25 ± 17
$\chi^2_{\rm r}$ Const.	21	1.5	7.2	2.2
$\chi^2_{\rm r}$ Flare	2.7	—	2.9	1.2
$F_{\nu,0}$ (μJy)	980 ± 40	—	720 ± 40	360 ± 70
$\sigma_{\rm t}^{\rm flare}$ (min)	$13.8^{+1.0}_{-0.6}$	—	$21.5^{+3.3}_{-2.7}$	$5.6^{+2.0}_{-1.0}$
$F_{\nu,{\rm q}}$ (μJy)	190 ± 15	—	240 ± 11	25 ± 15
Peak $f_{\rm circ}$ (%)	66 ± 4	—	-62 ± 5	30 ± 20
Energy (erg)	1.1×10^{27}	—	8.0×10^{26}	2.2×10^{26}

NOTE.—The rows are (top to bottom), (1) average flux density over the entire observation, (2) average fraction of circular polarization over the entire observation, (3) reduced χ^2 assuming that each lightcurve can be fit with only a constant term, (4) reduced χ^2 when we include a flare, (5) flare peak flux density, (6) flare FWHM duration, (7) quiescent flux density, (8) fraction of circular polarization at the peak of the flare, and (9) total energy release in the flare, assuming that the flares peaked at 8.46 GHz.

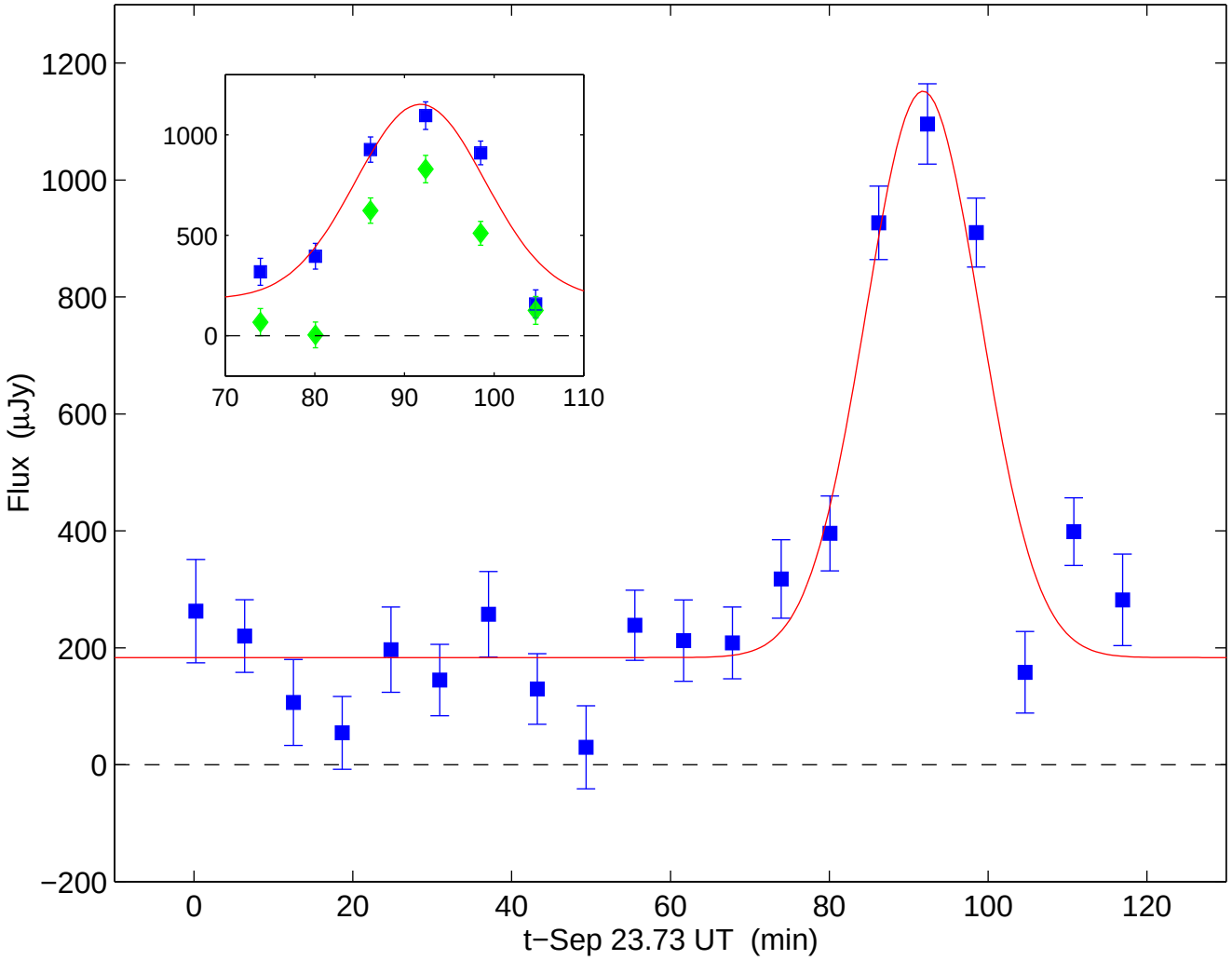

FIG. 1.— Lightcurve of the 8.46 GHz emission from TVLM 513 on 2001, Sep 23.73 UT, with 20 5.5-min bins. We find a single flare and persistent emission, which appears to be variable. The solid line is a Gaussian model (Equation 1). The inset shows the circularly polarized flux (diamonds) and the total flux (squares). The fraction of circular polarization near the peak of the flare is ≈ 65% (see Table 3).

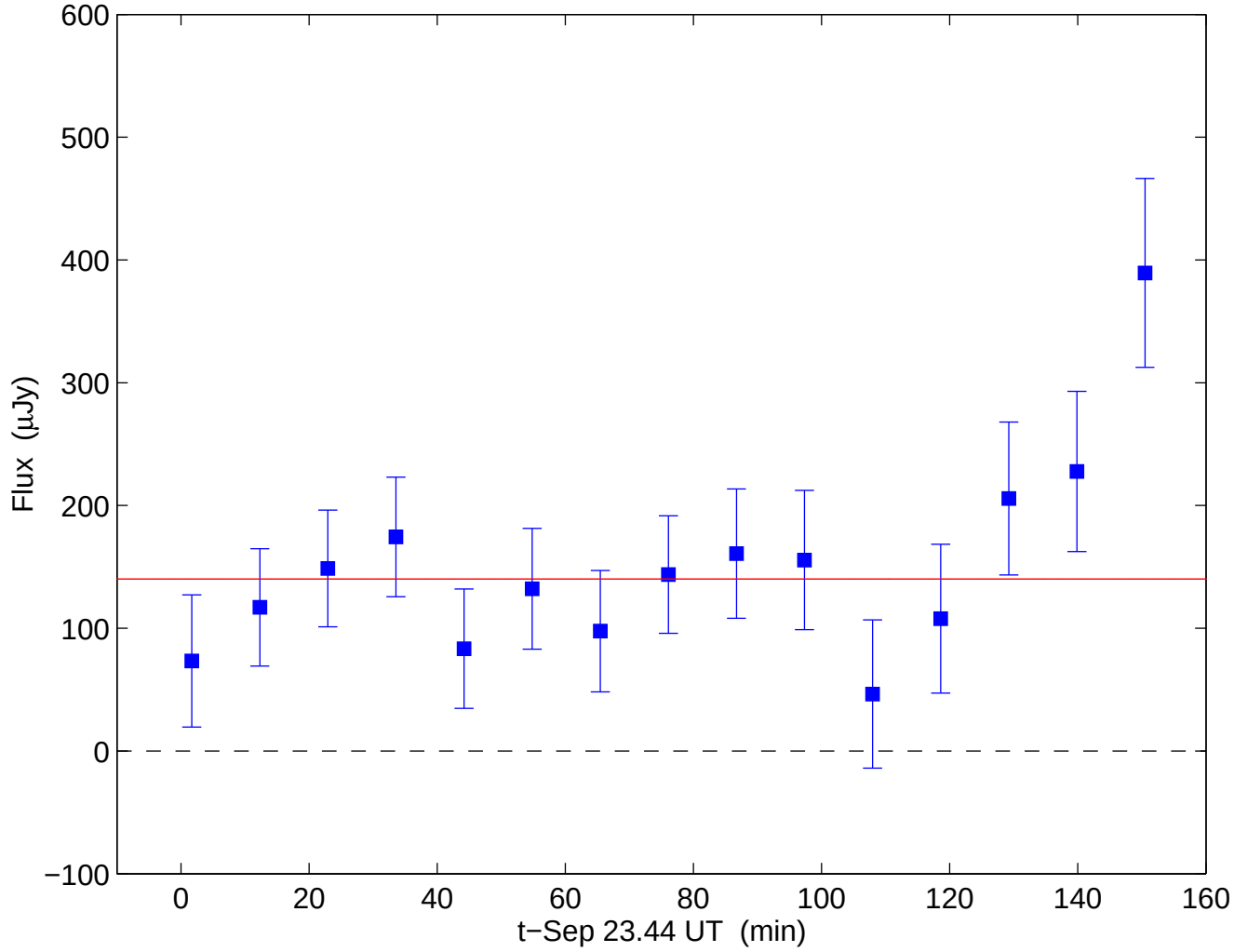

FIG. 2.— Lightcurve of the 8.46 GHz emission from 2MASS 0036+18 on 2001, Sep 23.44 UT, with 15 8.5-min bins. We find only persistent emission, with a marginal indication for re-brightening over the last thirty minutes of the observation. This possibly indicates the rise of a strong flare. The solid line is a fit to a constant source.

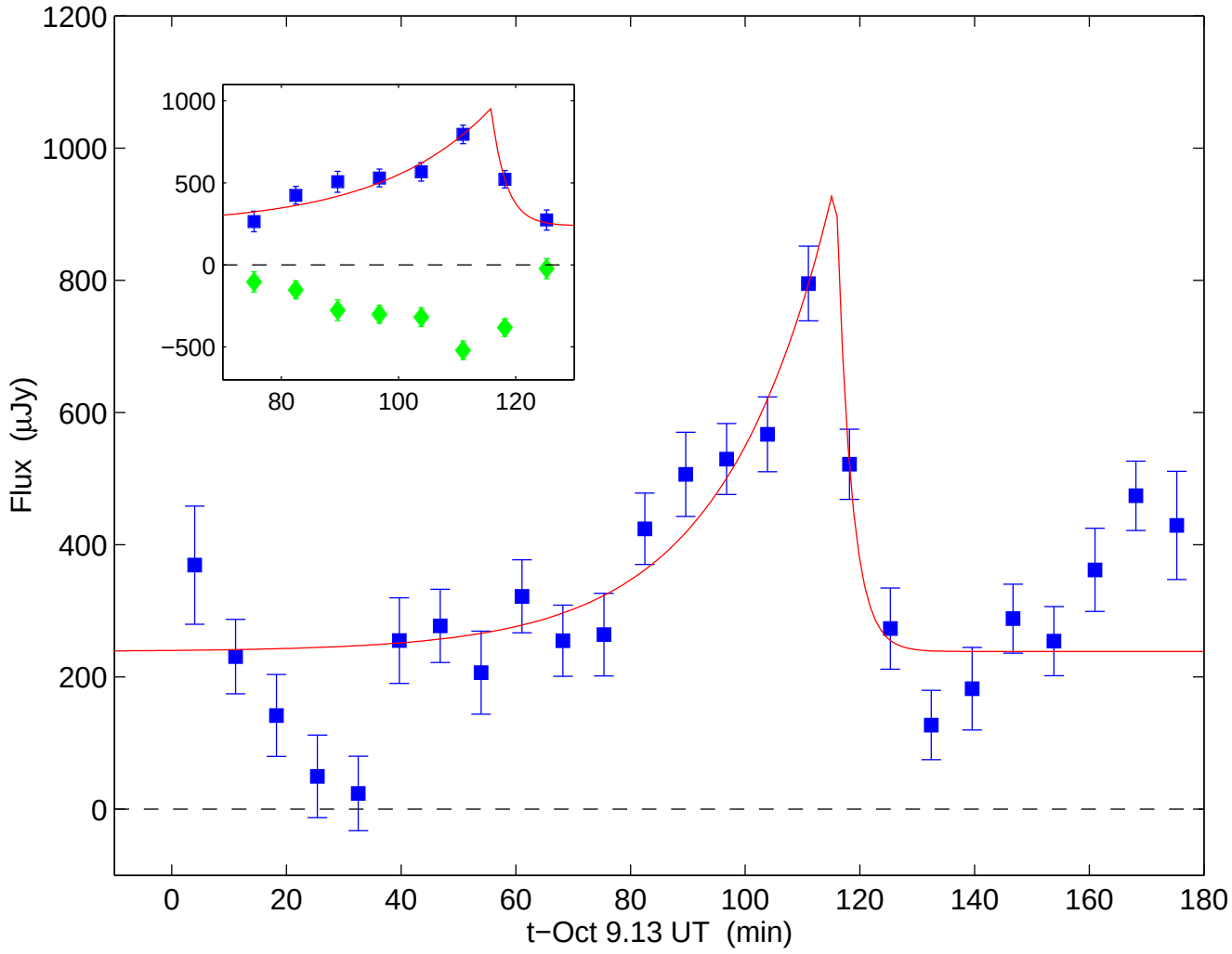

FIG. 3.— Lightcurve of the 8.46 GHz emission from 2MASS 0036+18 on 2001, Oct 9.13 UT, with 25 6.5-min bins. We find a flare and persistent emission, which appears to be strongly variable. The steep decline in flux during the first twenty minutes of the observation, and the shallow rise during the last sixty minutes possibly signal two additional strong flares. The solid line is an exponential model. The inset shows the circularly polarized flux (diamonds) and the total flux (squares). The fraction of circular polarization near the peak of the flare is $\approx -65\%$. The negative values indicate left-handed circular polarization (see Table 3).

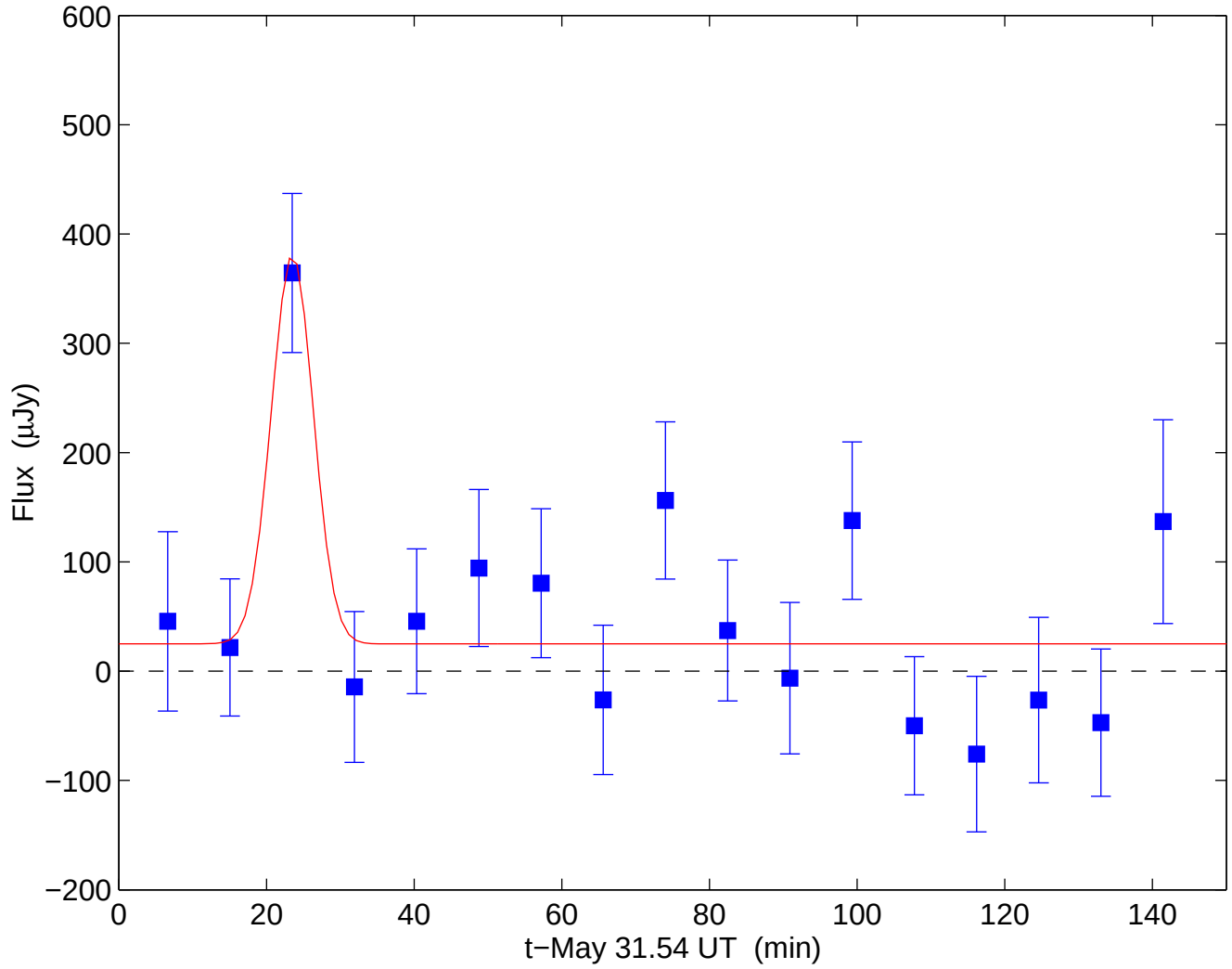

FIG. 4.— Lightcurve of the 8.46 GHz emission from BRI 0021 on 2001, May 31.54 UT, with 17 8-min bins. We find a single flare with a statistical significance of 4.5σ. The solid line is a Gaussian model (Equation 1). The fraction of circular polarization near the peak is $30 \pm 20\%$ (see Table 3).

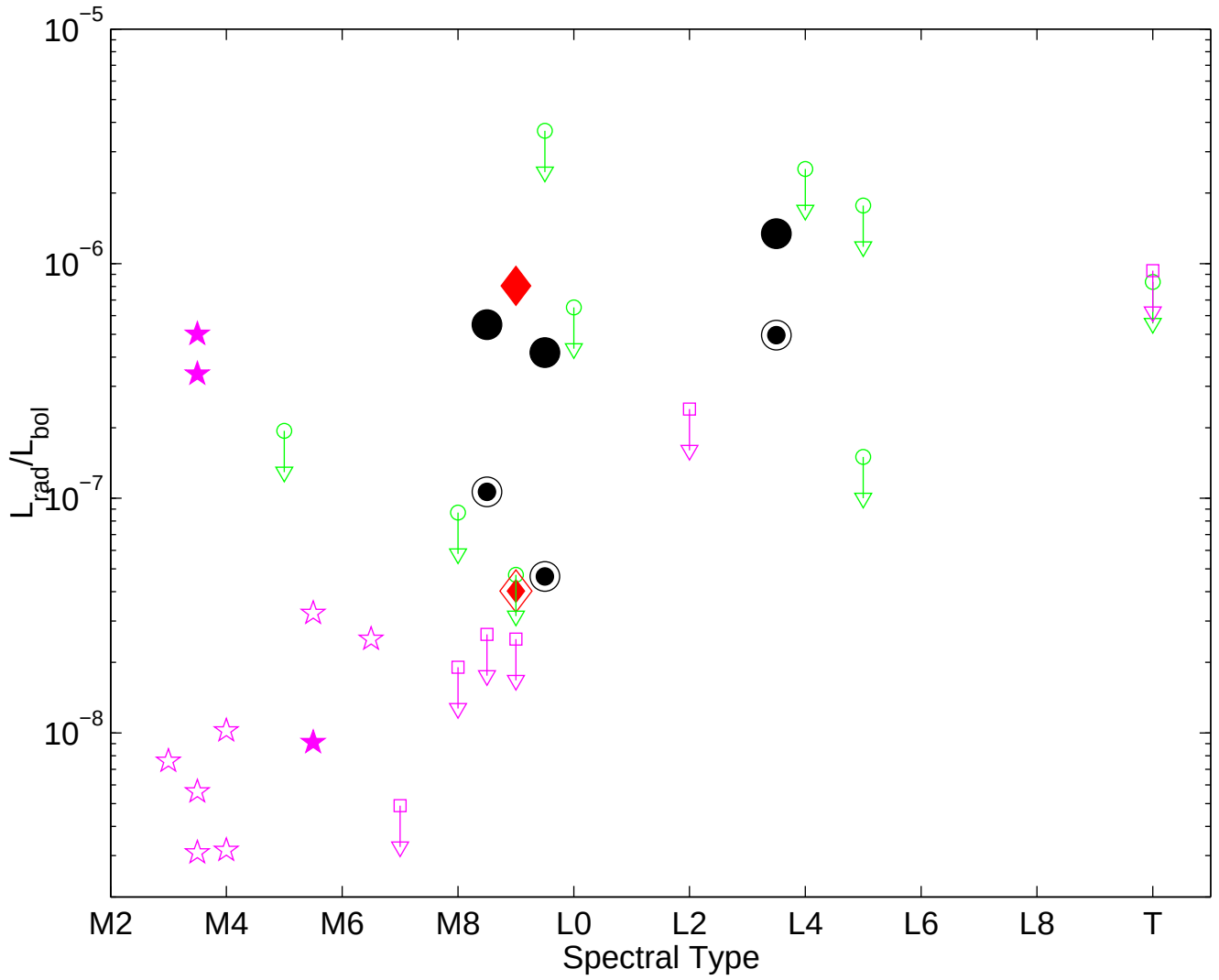

FIG. 5.— Ratio of flare luminosities (filled symbols) and persistent luminosities (open symbols and filled/open symbols) to bolometric luminosities vs. spectral type. Sources from this survey are designated by circles, LP 944-20 (B01) is designated by a diamond, the sources from Krishnamurthi, Leto & Linsky (1999) are designated by squares, and sources in the range M3-M6.5 (Cash, Charles & Johnson 1980; Pallavicini, Wilosn & Lang 1985; Leto et al. 2000; Stepanov et al. 2001) are designated by stars. The upper limits represent 3σ levels. When the bolometric luminosity of the source is not known, we estimated the value using other sources with the same spectral type (see Table 1). While the sample size is still small, it appears that there is no decline in radio activity between spectral types M3–L3.5, indicating that the radio and Hα emission are possibly decoupled.

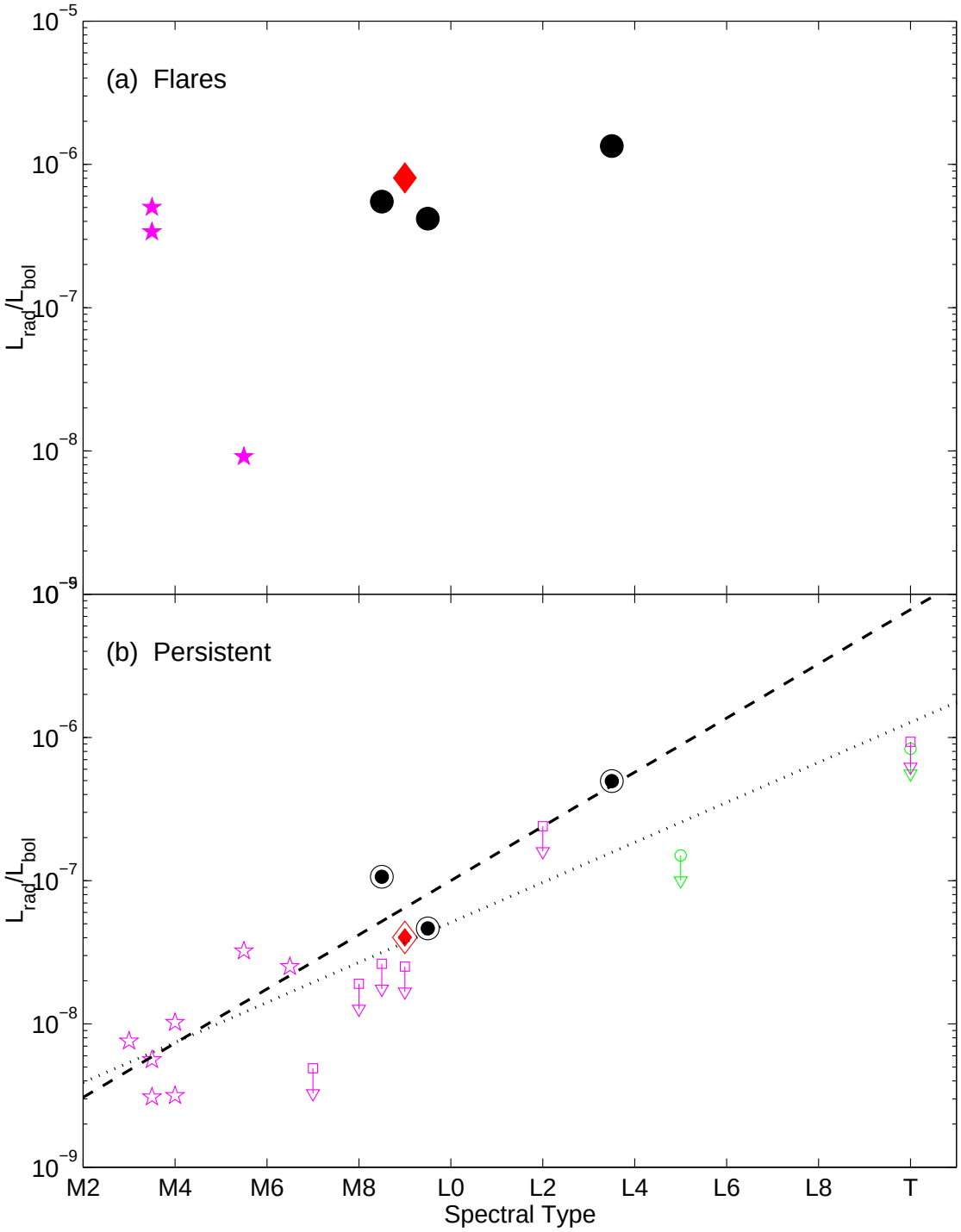

FIG. 6.— (a) Ratio of radio to bolometric luminosities for detected flares from M and L dwarfs. Symbols are as in Figure 5. With the exception of Proxima Centauri (M5.5), the radio activity appears to cluster around $\log(L_{\rm rad,f}/L_{\rm bol}) \approx -6$. This possibly indicates a saturation effect. (b) Ratio of radio to bolometric luminosities for persistent emission from the detected sources, and upper limits which are similar to or lower than these detections. The dashed line is a linear fit to the detections, while the dotted line includes the upper limits. In both cases there is an increase in $\log(L_{\rm rad,q}/L_{\rm bol})$ with spectral type. The same ratio for Hα emission drops significantly beyond M7. These observations indicate that the radio and Hα emission are probably uncorrelated at the bottom of the main sequence. The upper limits that violate the relation, and have measured rotational velocities, have $v\sin i < 10$ km sec^{-1}. This result is discussed in detail in §6 and Figure 7.

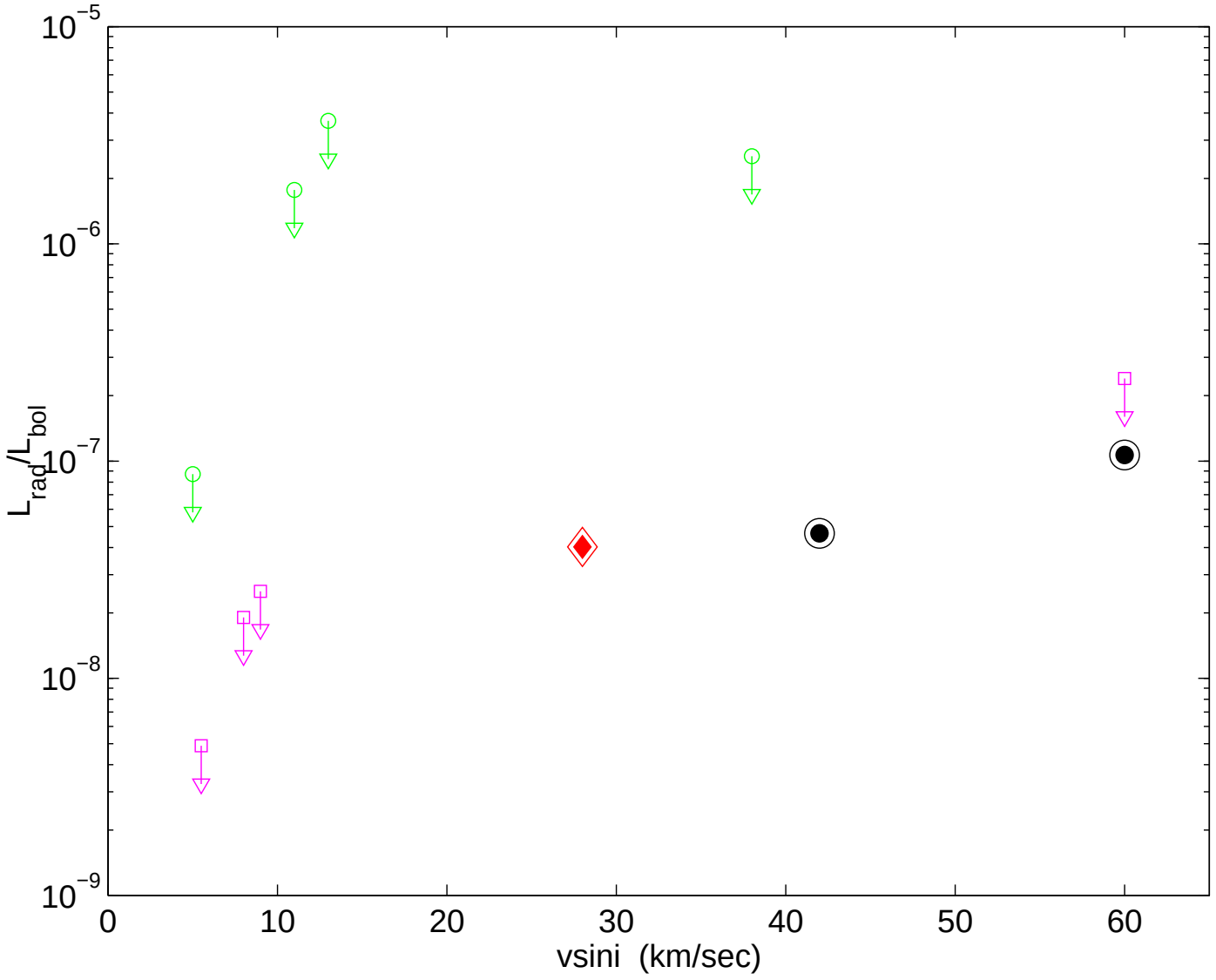

FIG. 7.— Ratios of persistent radio luminosity to bolometric luminosity for sources with measured rotational velocities. Symbols are as in Figure 5. The sources with detected radio emission have $v\sin i > 30$ km sec^{-1}, while sources which have upper limits lower than the detected levels have $v\sin i < 10$ km sec^{-1}. This trend is based on a small number of objects, but it provides tantalizing evidence for a correlation between radio activity and rotation.